Neuron
Article

An Unbiased Expression Screen for Synaptogenic Proteins Identifies the LRRTM Protein Family as Synaptic Organizers

Michael W. Linhoff,[1,2] Juha Laurén,[3,4] Robert M. Cassidy,[1] Frederick A. Dobie,[1] Hideto Takahashi,[1] Haakon B. Nygaard,[3] Matti S. Airaksinen,[4] Stephen M. Strittmatter,[3] and Ann Marie Craig[1,2,*]
[1]The Brain Research Centre and Department of Psychiatry, University of British Columbia, Vancouver, BC V6T 2B5, Canada
[2]Department of Anatomy and Neurobiology, Washington University School of Medicine, St. Louis, MO 63110, USA
[3]Departments of Neurology and Neurobiology, Yale University School of Medicine, New Haven, CT 06520, USA
[4]Neuroscience Centre, University of Helsinki, 00014 Helsinki, Finland
*Correspondence: amcraig@interchange.ubc.ca
DOI 10.1016/j.neuron.2009.01.017

SUMMARY

Delineating the molecular basis of synapse development is crucial for understanding brain function. Cocultures of neurons with transfected fibroblasts have demonstrated the synapse-promoting activity of candidate molecules. Here, we performed an unbiased expression screen for synaptogenic proteins in the coculture assay using custom-made cDNA libraries. Reisolation of NGL-3/LRRC4B and neuroligin-2 accounts for a minority of positive clones, indicating that current understanding of mammalian synaptogenic proteins is incomplete. We identify LRRTM1 as a transmembrane protein that induces presynaptic differentiation in contacting axons. All four LRRTM family members exhibit synaptogenic activity, LRRTMs localize to excitatory synapses, and artificially induced clustering of LRRTMs mediates postsynaptic differentiation. We generate *LRRTM1*$^{-/-}$ mice and reveal altered distribution of the vesicular glutamate transporter VGLUT1, confirming an in vivo synaptic function. These results suggest a prevalence of LRR domain proteins in *trans*-synaptic signaling and provide a cellular basis for the reported linkage of LRRTM1 to handedness and schizophrenia.

INTRODUCTION

Chemical synapses represent the principal means of communication between neurons. While significant progress has been made in determining the developmental signals that guide axons to their targets, the molecular mechanisms that determine the final establishment of circuits remain incompletely understood. Synapses are asymmetric cellular junctions composed of a presynaptic vesicle release site, a synaptic cleft, and a specialized postsynaptic receptive apparatus. A major challenge in elucidating the mechanisms that govern synapse formation and maturation is the enormous variety of synapse types in the mammalian brain. It is likely that this diversity requires contribution from a large number of molecular signals. In addition to neuronal transmembrane proteins, secreted factors such as FGFs and neuronal pentraxins, and glial-derived factors such as thrombospondin and complement cascade proteins shape synapse development (Stevens et al., 2007; Waites et al., 2005).

Significant attention has focused on the role of synaptic cell adhesion molecules (CAMs) in synapse development (Ackley and Jin, 2004; Dalva et al., 2007; Ko and Kim, 2007; Yamagata et al., 2003). Given the potential for a *trans*-synaptic interaction that could bridge the presynaptic release apparatus with the postsynaptic density, Scheiffele and colleagues tested whether neuroligin expressed in transfected HEK cells could assemble presynaptic terminals when cocultured with axons from pontine explants. Indeed, expression of neuroligin in HEK cells induced the clustering of synaptic vesicles in contacting axons (Scheiffele et al., 2000), via direct interaction with neurexins. In a parallel fashion, expression of β-neurexin in COS cells induces postsynaptic differentiation in contacting dendrites (Graf et al., 2004). These results show that a single molecular interaction can organize many aspects of presynaptic and postsynaptic assembly. Further studies indicate selective roles of different neuroligin and neurexin splice isoforms at excitatory versus inhibitory synapses (Chubykin et al., 2007; Craig and Kang, 2007). Moreover, analyses of knockout mice indicate an essential role for neurexins and neuroligins in synapse development (Missler et al., 2003; Varoqueaux et al., 2006). Neuroligin-1, -2, -3 triple-knockout mice die at birth due to defects in excitatory and inhibitory transmission, although single-neuroligin knockouts have only subtle phenotypes (Chubykin et al., 2007; Jamain et al., 2008; Varoqueaux et al., 2006).

The fibroblast-neuron coculture assay has proven to be a useful tool in testing candidate proteins for a role in synaptic development (Biederer and Scheiffele, 2007; Craig et al., 2006). Coculture assays have revealed synaptogenic activity for four families of neuronal CAMs, and in some cases their binding partners: neuroligins and partner neurexins, SynCAMs/Necls (Biederer et al., 2002), EphBs and partner ephrinBs (Aoto et al., 2007; Kayser et al., 2006), and netrin G ligands (NGLs/LRRC4s) (Kim et al., 2006). Knockout mice studies have validated roles for

EphBs/ephrinBs (Aoto et al., 2007; Henderson et al., 2001; Henkemeyer et al., 2003; Kayser et al., 2006) as well as neurexins/neuroligins in synapse development. Evidence is accumulating that proteins testing positive for synaptogenic activity in this assay may not be essential for initiating the formation of or maintaining the integrity of synaptic junctions. Rather, these factors may serve a role in the maturation of the synapse, recruiting components necessary for synaptic function.

Here we used the fibroblast-neuron coculture assay to search for novel synaptogenic proteins. We created and screened a set of full-length size-selected cDNA expression libraries from developing rat brain. Screening to date reveals a prevalence of leucine-rich repeat (LRR) synaptogenic proteins arising from this unbiased approach. We identify the leucine rich repeat transmembrane neuronal (LRRTM) protein family as able to instruct excitatory presynaptic differentiation and to mediate postsynaptic differentiation. Furthermore, we generate an LRRTM1 knockout mouse and reveal a modest synaptic phenotype, suggesting a synaptic basis for the recently reported linkage of LRRTM1 to handedness and schizophrenia (Francks et al., 2007). Parts of this work have previously been published in doctoral dissertations (Linhoff, 2008; Lauren, 2007).

RESULTS

Expression Screening for Molecules Involved in Presynaptic Differentiation

To test the feasibility of converting the fibroblast-neuron coculture assay into an expression screen, neuroligin-1 and neuroligin-2 cDNAs were diluted up to 1:1000 with either a soluble CFP expression plasmid or a pool of inactive cDNAs. Neuroligin-2 could be diluted 500-fold while still consistently yielding a positive synaptogenic signal on a single neuron-COS cell coculture coverslip, while neuroligin-1 could only be diluted 100-fold (data not shown). Thus, a pool size of ~250 clones would be likely to yield novel clones with synaptogenic activity of similar potency as neuroligins. This pool size of 250 is considerably smaller than typical pool sizes of 1,000 - 10,000 used for expression screens involving more sensitive detection technologies (e.g., Fournier et al., 2001). Furthermore, since we are expecting active proteins to be transmembrane or secreted, positive clones would have to be full-length to contain the signal peptide essential for proper trafficking.

Thus, the first step in the screen was to generate an unamplified cDNA expression library with a high percentage of full-length clones (Figure 1A). We isolated mRNA from rat forebrain at P11, the peak of synaptogenesis (Micheva and Beaulieu, 1996). To ensure representation of full-length molecules, we used the biotinylated cap-trapper method that had been developed for large-scale sequencing projects (Figures S1A and S1B) (Carninci et al., 1996). The resultant cap-trapped cDNA was subjected to rigorous size fractionation, and individual unamplified libraries were maintained. Mean insert size of the resultant libraries was confirmed by restriction digestion (Figure S1C), and sequencing of over 50 clones indicated that all contained the 5′ ATG. We were successful in creating high-quality expression libraries for inserts up to 5 kb using pcDNA3.1 as the host expression vector (Figure 1A).

Figure 1B illustrates the protocol that we used for the screen to identify cDNA pools that contained synaptogenic activity. Synaptogenic activity was assayed by the immunocytochemical detection of experimentally induced hemisynapses. The cocultures were immunostained with synapsin I antibody to detect synaptic vesicle clustering at contact sites between COS cells and axons. Coimmunostaining for the postsynaptic markers PSD-95 family and gephyrin ensured that synapsin immunoreactivity associated with bona fide interneuronal synapses was not counted as a false positive. A cDNA pool was considered positive if it generated any COS cell with significant associated synapsin clusters unapposed to PSD-95 family or gephyrin. We screened positive cDNA pools using PCR to detect known synaptogenic factors. The first positive pool, PD026, was found in the 4–5 kb library, tested positive for neuroligin-2 using PCR, and was not fractionated to isolate the single responsible synaptogenic cDNA. Further screening within the 3–4 kb library resulted in another positive pool, PC064, which tested PCR negative for neuroligins. We subdivided the PC064 cDNA pool to isolate the synaptogenic clone. Generation of arrayed clones and DNA from a positive subpool aided in identifying the active clone. The isolated clone, PC064-89-29-40 (pool PC064, subpool 89, subpool 29, clone 40), was identified as leucine-rich repeat transmembrane protein LRRTM1. The LRRTM protein family consists of four members, each possessing ten extracellular leucine-rich repeats, a single transmembrane domain, and an ~70 amino acid cytoplasmic domain (Figures 1B and S2) (Lauren et al., 2003).

Quantitation of the Synaptogenic Activity for LRRTM Family Members

We cloned each of the LRRTM family members from rat cDNA, fused CFP to the C terminus, and tested each protein for synaptogenic activity in the coculture assay. N-cadherin has been shown previously to not induce presynaptic clustering (Scheiffele et al., 2000); we confirmed this (see below) and used N-cadherin as a negative control. As an additional control, we used the LRR protein, AMIGO, which has been shown to interact with the axons of hippocampal neurons and induce neurite outgrowth and fasciculation (Kuja-Panula et al., 2003).

To obtain a quantitative measure of each protein's ability to instruct presynaptic differentiation, we measured the amount of synapsin clustering associated with transfected COS cells and not associated with MAP2-positive dendrites to exclude interneuronal synapses. Robust synaptogenic activity was observed for LRRTM1-CFP, LRRTM2-CFP, LRRTM4-CFP, and neuroligin-2-CFP (Figures 2A, 2B, and S3B). In some instances clustering of the CFP fusion protein could be observed apposed to synapsin puncta (Figures 2A and 2B, insets). LRRTM3-CFP consistently yielded limited activity in the coculture assay (Figure S3A). In contrast to the LRRTMs, synaptogenic activity was not observed for N-cadherin-CFP or the LRR-containing AMIGO-CFP (see Figure 2C for images of AMIGO-CFP). LRRTM1-CFP, LRRTM2-CFP, LRRTM4-CFP, and neuroligin-2-CFP each induced a >14-fold increase in synapsin clustering when compared to results obtained from N-cadherin-CFP or AMIGO-CFP-transfected cells (Figure 2D, $n = 20$ transfected COS cells per construct; ANOVA $p < 0.0001$; t test versus

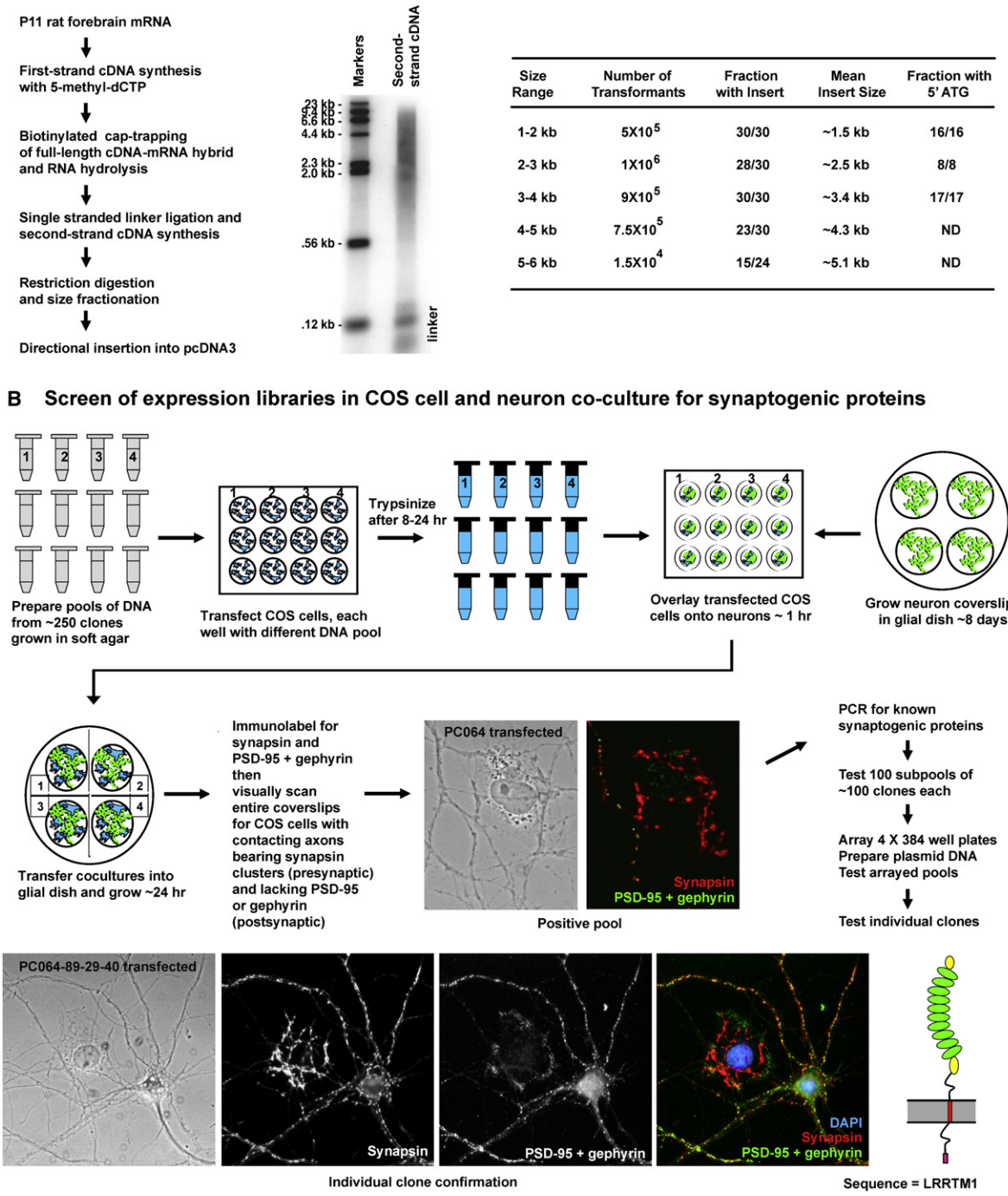

Figure 1. Expression Screening Identifies LRRTM1 as a Synaptogenic Factor

(A) Construction of cDNA expression libraries. Flow diagram summarizes the procedure. The autoradiograph in the center shows the size range of the second-strand cDNA product. Characteristics of the libraries are summarized in the table.

(B) Flow diagram illustrating the experimental protocol of the expression screen leading to the discovery of LRRTM1. Expression library pools were minimally amplified in soft agar and plasmid DNA prepared and transfected into COS cells in a 12-well tissue culture plate. Transfected COS cells were seeded onto neuron coverslips, and the coculture coverslips were transferred back into the astrocyte feeder dish. After ~24 hr, coculture coverslips were fixed, immunolabeled, and scanned visually on a fluorescent microscope. Images are shown from the original pool, PC064, that scored as positive and was later found to contain LRRTM1. Synaptogenic activity is indicated by the presence of synapsin clusters (red) on axons contacting a COS cell; these presumed induced clusters did not label for postsynaptic markers PSD-95 family plus gephyrin (green), unlike the endogenous neighboring synapses on dendrites. This pool tested negative for PCR tests for

N-cadherin-CFP and AMIGO-CFP $p < 0.005$). In contrast, synapsin clustering associated with LRRTM3-CFP was 1.6- to 3.3-fold above that associated with N-cadherin-CFP or AMIGO-CFP (t test versus N-cadherin and AMIGO $p < 0.05$). In separate experiments to confirm the lack of presynaptic inducing activity of N-cadherin compared with no surface protein expression, we compared the percentage of cells exhibiting any clusters of synapsin not associated with PSD-95 or gephyrin for COS cells expressing N-cadherin-CFP (1.6% ± 0.3%) or expressing CFP (1.8% ± 0.5%; $p > 0.1$).

Axonal contact area determined from dephospho-tau immunoreactivity was also higher for LRRTM2-CFP, LRRTM4-CFP, and neuroligin-2-CFP than for N-cadherin-CFP or AMIGO-CFP (Figure S3C; ANOVA $p < 0.0001$), suggesting an effect on axon adhesion as well as presynaptic differentiation. The less than 2-fold increase in axon contact area for LRRTM2-CFP or LRRTM4-CFP was not sufficient to explain the >14-fold increase in synapsin clustering, indicating a direct presynaptic effect. Thus, measures of synapsin area normalized per axon contact area also revealed significant induction of presynaptic differentiation by LRRTMs (Figure 2E). Although the most synaptogenic factors tended to have increased axon contact area, the same phenomenon did not hold true for LRRTM1-CFP. This result is likely due to the reduced surface expression of LRRTM1 relative to the other family members. We observed that LRRTM1 accumulates extensively in the endoplasmic reticulum of transfected nonneuronal cells (data not shown), and this result has been observed previously (Francks et al., 2007).

Since synapsin is a vesicle-associated protein, we also tested for other markers of presynaptic differentiation. LRRTMs induced clustering of the active zone cytomatrix protein bassoon (Figures S4A–S4D), as well as the integral synaptic vesicle membrane protein synaptophysin (Figures S4E–S4H).

LRRTMs Instruct Excitatory Presynaptic Differentiation

We tested whether the synaptogenic activity was restricted to excitatory or inhibitory presynaptic differentiation. The CFP fusion proteins were scored blind for significant clustering of the presynaptic vesicular neurotransmitter transporters, VGLUT1 and VGAT, to identify excitatory or inhibitory presynaptic differentiation, respectively. Significant clustering of VGLUT1 unapposed to PSD-95 family was observed for LRRTM1-CFP, LRRTM2-CFP, LRRTM3-CFP, LRRTM4-CFP, and neuroligin-2-CFP (Figures 2F–2J; ANOVA $p < 0.0001$; t test versus N-cadherin-CFP and AMIGO-CFP $p < 0.0005$). In contrast, only LRRTM2-CFP and neuroligin-2 showed robust clustering of VGAT unapposed to gephyrin (Figures S3D–S3F; ANOVA $p < 0.0001$).

LRRTM Instructs the Development of Functional Glutamate Release Sites

Since LRRTM1 and LRRTM2 demonstrated the most potent synaptogenic activity of the four family members, we focused further efforts on these two family members. To test whether the induced presynaptic clusters were functional for release, we used whole-cell patch voltage clamp to record currents from HEK293T cells cotransfected with LRRTM2-CFP and NMDA receptor subunits YFP-NR1 and NR2A and cocultured with hippocampal neurons. A similar assay was used to show that neuroligin-1 coexpressed with NMDA receptors could induce excitatory postsynaptic current (EPSC)-like events in HEK cells cocultured with cerebellar granule neurons (Fu et al., 2003). Here, bursts of spontaneous activity much like NMDA receptor currents typical of cultured neurons were recorded from the HEK293T cells expressing LRRTM2-CFP and NMDA receptors (Figure 3A). These bursts of high-amplitude events were abolished by tetrodotoxin (TTX) and reduced to miniature EPSC-like events, indicating that the bursts arise from action-potential-dependent neuronal network activity that drives glutamate release onto the transfected cell. In contrast, HEK293T cells cotransfected with YFP-NR1, NR2A, and N-cadherin-CFP as a negative control exhibited only rare spontaneous events and lacked the bursting activity observed for LRRTM2-CFP-expressing cells (Figure 3B). These rare synaptic-like events may correspond to fusion of immature synaptic vesicles or may arise from orphan release sites of axons (Krueger et al., 2003). The frequency and amplitude of events onto N-cadherin-expressing cells was not significantly altered by TTX. Amplitude of events onto LRRTM2-CFP-expressing cells was reduced 4.6-fold by TTX ($n = 5$ cells with frequency >0.1 Hz), indicating the formation of multiple functional release sites. Quantitative analysis confirmed a greater than 20-fold overall increase in frequency of spontaneous EPSC-like events and 6.6-fold increase in frequency of miniature EPSC-like events in HEK293T cells expressing LRRTM2-CFP compared with N-cadherin-CFP-expressing cells (Figure 3C; $n \geq 10$, $p < 0.005$ t test). The amplitude of spontaneous but not miniature events was also significantly increased for LRRTM2-CFP versus N-cadherin-CFP-expressing cells (Figure 3D; $p < 0.05$ t test comparison of mean cell values). Mean amplitude of miniature events was 89 and 99 pA for N-cadherin or LRRTM2-CFP-expressing cells, respectively, suggesting that sufficient levels of diffuse surface NMDA receptors were obtained in the HEK cells to provide a sensitive assay of release. All synaptic-like events were abolished by NMDA receptor antagonist APV (data not shown). Thus, the presynaptic specializations induced by LRRTM2 expression are functional with respect to evoked and spontaneous glutamatergic synaptic vesicle exocytosis.

The LRR Domain of LRRTM Is Necessary and Sufficient for Synaptogenic Activity

To determine if the LRR domain was necessary for synaptogenic activity, a deletion mutant lacking the LRR domain, ΔLRR-LRRTM2-CFP, was tested in the coculture assay. The deletion mutant was expressed on the cell surface, but presynaptic differentiation was not observed in axons that contacted the surface of transfected COS cells (Figure S5). To determine whether the LRR domain of LRRTM2 is sufficient to instruct presynaptic

known synaptogenic proteins and was further broken down. Sequence analysis revealed the single active clone to be rat LRRTM1. The final cartoon illustrates LRRTM domain structure. LRRTMs contain ten extracellular leucine-rich repeats (green) flanked by N- and C-terminal disulfide bonded "capping" domains (yellow), a single-pass transmembrane domain (red), and a potential PDZ ligand (magenta).

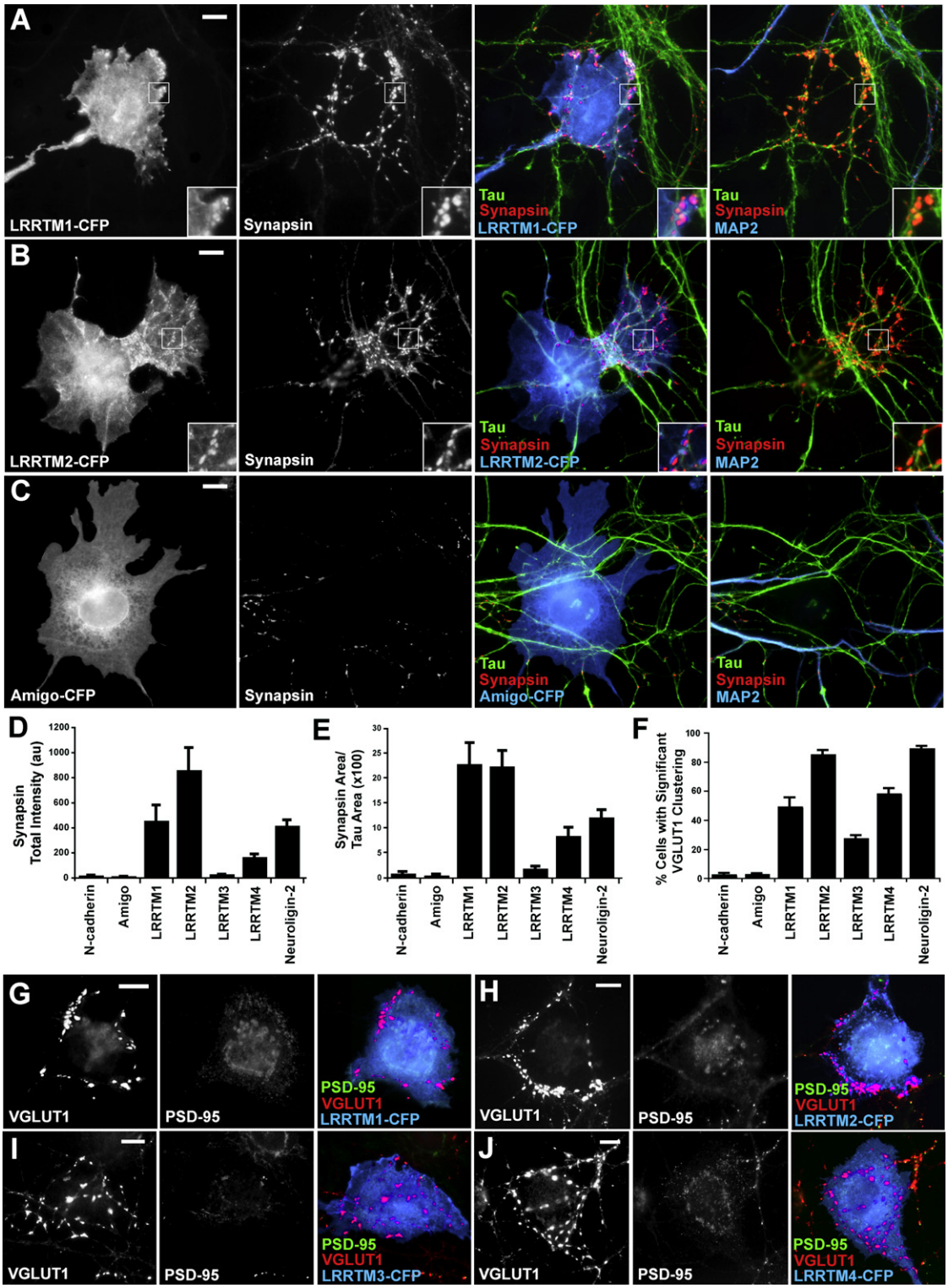

Figure 2. Quantitation of the Synaptogenic Activity of LRRTM Family Members

(A–E) COS cells were transfected with C-terminal CFP fusion proteins, cocultured with hippocampal neurons, and the clustering of synapsin was quantitated at sites where hippocampal axons contacted transfected cells and not dendrites. (A and B) Synapsin clustering is observed along axons (labeled with dephosphorylated tau) contacting COS cells expressing LRRTM1-CFP or LRRTM2-CFP and lacking contact with dendrites (labeled with MAP2). The insets show apposition of LRRTM-CFP clusters in the COS cells and synapsin clusters in contacting axons. (C) No significant synapsin clustering is evident along axons contacting

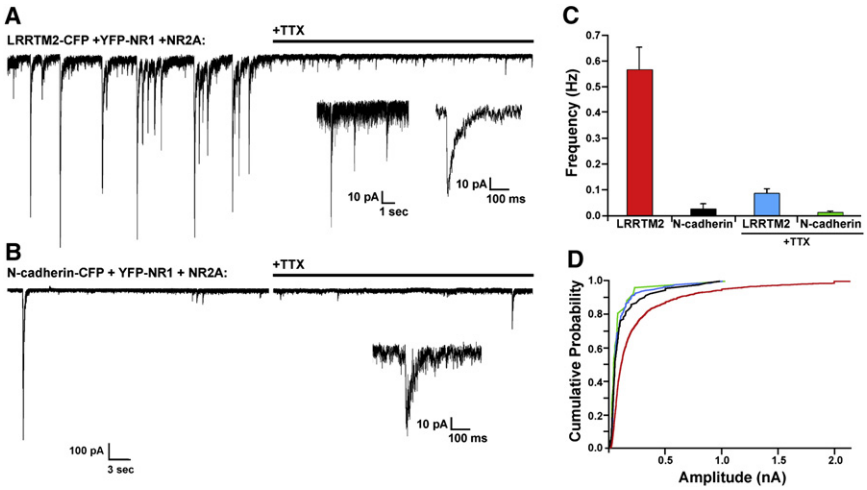

Figure 3. LRRTM Instructs Assembly of Functional Vesicle Release Sites

HEK cells were cotransfected with LRRTM2-CFP and the NMDA receptor subunits, YFP-NR1 and NR2A. A similar cotransfection was performed with N-cadherin-CFP and NMDA receptor subunits as a negative control. The transfected HEK cells were cocultured with hippocampal neurons for ~24 hr before recording.

(A) Representative trace from whole-cell recording of a HEK cell cotransfected with LRRTM2-CFP and NMDAR. Spontaneous synaptic-like currents can be seen. TTX abolished this bursting activity, leaving miniature EPSC-like events. The inset shows sample miniature EPSC-like events and an average of such events from one cell.

(B) Trace from whole-cell recording of one of the most active HEK cells cotransfected with N-cadherin-CFP and NMDAR. Only occasional isolated events were observed in the absence or presence of TTX; inset shows a sample event in the presence of TTX.

(C) Frequency plot of EPSC-like events comparing LRRTM2-CFP and N-cadherin-CFP transfected HEK cells in the absence and presence of TTX. Number of cells recorded: LRRTM2 (22), N-cadherin (17), LRRTM2 + TTX (11), N-cadherin + TTX (10).

(D) Cumulative probability plot of current amplitude for the four conditions shown in panel (C).

All error bars are SEM.

differentiation, a fusion protein of the LRR domain of LRRTM2 with a myc-epitope tagged placental alkaline phosphatase (AP), LRRTM2 LRR-AP, was linked via biotinylated anti-myc antibody onto neutravidin beads. Contact of these LRR-AP-coated beads with isolated axons of hippocampal neurons induced clustering of synapsin or VGLUT1 at contact sites (Figures 4A and 4B, right panels). Beads coated with the control AP protein did not display synaptogenic activity (Figures 4A and 4B, left panels). Random counts revealed synapsin clustering at 34.1% of LRR-AP bead contacts and only 2.1% of control AP bead contacts (n = 50 fields). The mean synapsin intensity under all LRR-AP beads was 6.3-fold higher than that under control AP beads ($p < 0.0001$). Clustering of the active zone marker bassoon could also be detected at LRR-AP bead-axon contact sites. In fact, there appeared to be separation between the bassoon-labeled active zone and the VGLUT1-positive vesicle pool, with the active zone most closely apposed to the bead surface (Figure 4B, right panel, inset). The LRR-AP beads did not appear to cluster VGAT at contact sites with GAD-positive axons (data not shown). These results show that the LRR domain of LRRTM2 is necessary and sufficient to induce excitatory presynaptic differentiation without any contribution from other factors.

Localization of Recombinant LRRTMs to Excitatory Synapses Independently of the PDZ Domain Binding Site

To begin to assess subcellular localization, we created extracellular YFP fusions of LRRTM1 and LRRTM2 and transfected hippocampal neurons in culture. YFP-LRRTM-1 or -2 expressed at low level in hippocampal neurons traffic to dendrites and assume a punctate, synaptic-like pattern (Figures 5A–5C). YFP-LRRTM-1 or -2 colocalized with PSD-95 family proteins opposite VGLUT1 puncta. YFP-LRRTM-1 and -2 appeared to be exclusively colocalized with the excitatory postsynaptic scaffolding proteins of the PSD-95 family but not with the inhibitory postsynaptic scaffolding protein gephyrin. Quantitation of thresholded puncta revealed 72.6% overlap of YFP-LRRTM2 puncta with PSD-95 family, compared with 4.5% overlap of mirror images as control, and 8.0% overlap with gephyrin. These results suggest that the function of LRRTMs may be restricted to glutamatergic and not GABAergic hippocampal synapses, although more definitive tests and more diverse contexts are required.

The C terminus of all four LRRTM members ends in a pattern of residues (-E-C-E-V) that resembles the X-S/T-X-V Class I PDZ domain ligand pattern (Sheng and Sala, 2001). Furthermore, a glutamate at the −3 position is preferred for PDZ domains 1 and 2 of PSD-95, for which several natural ligands terminate

AMIGO-CFP expressing COS cells. The only synapsin clusters occur at axon-dendrite contacts, at endogenous synapses. (D) Quantitation of the total integrated intensity of synapsin staining associated with COS cells transfected with the indicated CFP fusion proteins and not associated with MAP2. (E) Quantitation of the total synapsin pixel area associated with COS cells transfected with the indicated CFP fusion proteins divided by the tau-positive axon contact area. ANOVA $p < 0.0001$ for (D) and (E). Scale bar, 10 μm.

(F–J) COS cells expressing LRRTM-CFP fusion proteins and cocultured with hippocampal neurons clustered the specific glutamatergic presynaptic marker VGLUT1 at nonsynaptic sites in contacting axons. (F) For quantitating VGLUT1 clustering, individual transfected COS cells were scored as either positive or negative; 100 cells were assayed per coverslip, and four coverslips were analyzed for each recombinant protein. ANOVA $p < 0.0001$. (G–J) Expression of LRRTM1-CFP (G), LRRTM2-CFP (H), LRRTM3-CFP (I), or LRRTM4-CFP (J) results in VGLUT1 clustering on axons contacting the expressing COS cell and not associated with PSD-95-family proteins. This is a greater level of clustering than is generally seen for LRRTM3. Scale bar, 10 μm.

All error bars are SEM.

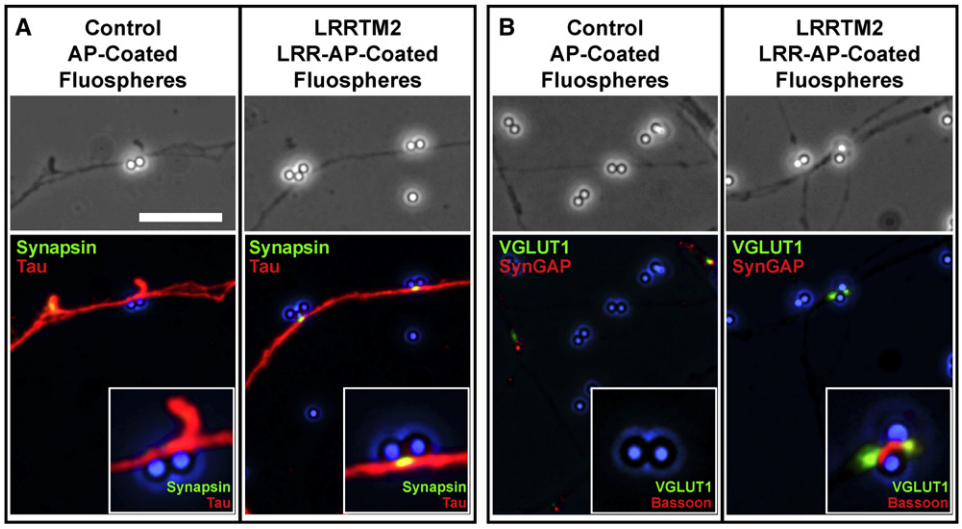

Figure 4. The LRR Domain of LRRTM Instructs Presynaptic Differentiation

(A) Right panel: clustering of synapsin was observed at sites where axons contacted beads coated with LRRTM2 LRR-AP. Left panel: no clustering was observed at sites where axons contacted control beads coated with control AP protein. Top panel: phase contrast; bottom panel with inset: synapsin immunostaining was used to detect presynaptic differentiation, tau labels axons, and the phase contrast bead image is merged in the blue channel.

(B) Right panel: clustering of VGLUT1 was observed at sites where axons contacted beads coated with LRRTM2 LRR-AP. Left panel: no clustering was observed at the axon-contact site with control beads. Top panel: phase contrast; bottom panel: immunostaining for SynGAP was used to detect endogenous synapses, and VGLUT1 immunostaining was used to detect excitatory presynaptic differentiation. In the inset, bassoon and VGLUT1 immunostaining show the separation of the synaptic vesicle pool and the active zone at the site of axon contact with beads (phase-contrast image placed in blue channel). Scale bar, 10 μm.

in -E-S/T-D-V (Sheng and Sala, 2001). Although a cysteine has not been reported in the −2 position for PDZ domain ligands, the similarity prompted us to test whether LRRTMs might bind PSD-95. We tested whether YFP-LRRTM2 could colocalize with PSD-95 in COS cells. YFP-LRRTM2 frequently forms small clusters in transfected COS cells. When PSD-95-mRFP was co-transfected with YFP-LRRTM2, the two proteins colocalized precisely in larger discrete aggregates (Figure 5D). Similar co-clustering has been observed for coexpressed PSD-95 and other ligands and is thought to reflect the formation of large complexes via multimerization of PSD-95 and binding to ligand. Deletion of the C-terminal E-C-E-V residues of YFP-LRRTM2 disrupted the colocalization with PSD-95 (Figure 5E). We also confirmed the interaction by coimmunoprecipitation of myc-tagged PSD-95 with YFP-LRRTM2 coexpressed in COS cells (Figure 5F). Again, deletion of the C-terminal E-C-E-V residues of YFP-LRRTM2 resulted in loss of the interaction. Thus, LRRTM2 can interact with PSD-95 via its C-terminal E-C-E-V. However, we were unable to coimmunoprecipitate LRRMT2 and PSD-95 family proteins from rodent brain (data not shown). The major in vivo interacting partner for LRRTM2 may be a different PDZ domain protein, or interaction with the PSD-95 family may be regulated in vivo, perhaps via modification of the −2 cysteine.

To determine whether the PDZ domain binding site is essential for postsynaptic clustering of LRRTMs, we again assessed localization of YFP-LRRTM2 constructs in cultured neurons. Deletion of the C-terminal E-C-E-V did not abolish clustering of YFP-LRRTM2ΔPDZ at glutamate postsynaptic sites colocalizing with PSD-95 (Figures 5G and 5H). However, deletion of the C-terminal 55 residues leaving only 17 residues after the transmembrane domain did abolish clustering of YFP-LRRTM2ΔC-term (Figure 5I). Deletion of this C-terminal domain also abolished polar distribution of the LRRTM2 protein, resulting in detection of the YFP-LRRTM2ΔC-term on the surface of axons as well as dendrites (Figure S6). Thus, the C terminus of LRRTM2 but not the specific PDZ domain binding site is required for postsynaptic clustering and for polarized distribution.

Overexpression of LRRTM in Neurons Increases Clustering of Presynaptic Antigens Via the Extracellular Domain

We wondered whether high-level expression of YFP-LRRTM2 in neurons might increase presynaptic clustering onto the expressing neurons, similar to effects in the COS cell cocultures. Indeed, high-level expression of YFP-LRRTM2 in neurons resulted in greatly enhanced clustering of bassoon and synapsin onto the expressing neurons in comparison with nontransfected neighbor neurons (Figure S6). Enhanced presynaptic clustering was also induced by YFP-LRRTM2ΔC-term and thus mediated by the extracellular domain of LRRTM2 (Figure S6). Although YFP-LRRTM2ΔC-term reached the surface of axons as well as dendrites, the enhanced presynaptic clustering was largely limited onto the somatodendritic domain, perhaps via other mechanisms promoting axon-dendrite contact over axon-axon contact.

Postsynaptic Differentiation Mediated by LRRTMs

We next determined whether LRRTMs may be able to mediate postsynaptic as well as induce presynaptic differentiation. We tested whether artificial clustering of LRRTMs at nonsynaptic sites on dendrites might result in coclustering of postsynaptic proteins. Hippocampal neurons were transfected to express low levels of

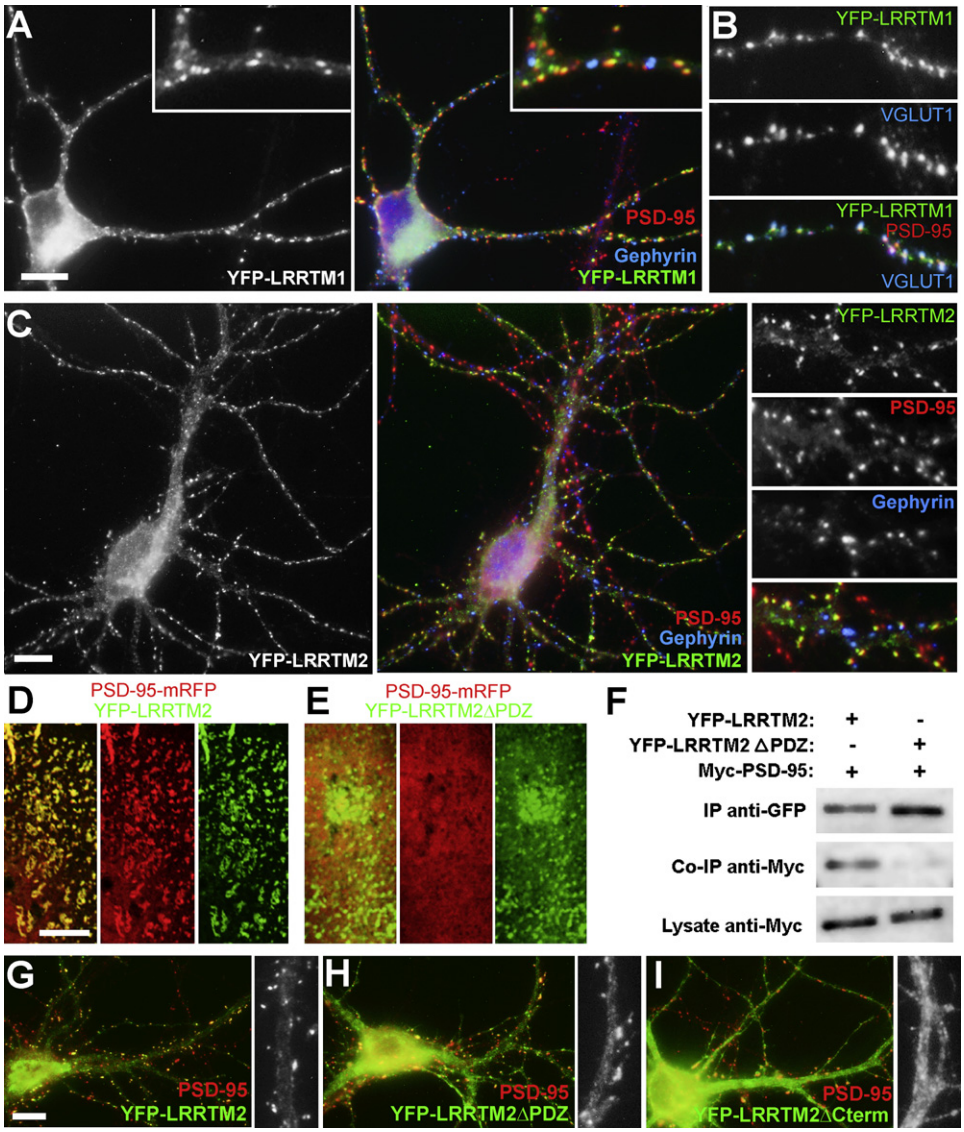

Figure 5. Recombinant LRRTMs Localize to Excitatory Postsynaptic Sites Independently of PDZ Domain Binding

(A–C) Hippocampal neurons were transfected at 8–9 DIV with YFP-LRRTM1 (A and B) or YFP-LRRTM2 (C), and the cultures were fixed 2–3 days after transfection. YFP-LRRTMs are localized to puncta in the dendrites of hippocampal neurons. YFP-LRRTM puncta colocalize with puncta of PSD-95 family excitatory postsynaptic proteins but not gephyrin inhibitory postsynaptic protein (A and C). YFP-LRRTMs were not observed in axons or at presynaptic sites; panel (B) shows YFP-LRRTM1 colocalized with PSD-95 family and apposed to VGLUT1. Scale bar, 10 μm.

(D–F) Recombinant LRRTM and PSD-95 interact in COS cells. (D) Confocal image of a COS cell cotransfected with YFP-LRRTM2 and PSD-95-mRFP. The two proteins form colocalized aggregates. (E) Confocal image of a COS cell cotransfected with YFP-LRRTM2ΔPDZ and PSD-95-mRFP. While YFP-LRRTM2ΔPDZ forms small clusters even when expressed alone, PSD-95 does not cocluster but remains diffusely localized. Scale bar, 10 μm. (F) Myc-tagged PSD-95 was cotransfected into COS cells with either wild-type YFP-LRRTM2 or YFP-LRRTM2ΔPDZ. Immunoprecipitation with anti-GFP antibody pulled down Myc-PSD-95 only when the full C terminus of LRRTM2 was present.

(G–I) Hippocampal neurons were transfected with recombinant YFP-LRRTM2 constructs as in panels (A)–(C). (G) Clustering of YFP-LRRTM2 at postsynaptic sites colocalizing with PSD-95 is again shown. (H) Deletion of the last four residues, the PDZ domain binding site, did not abolish synaptic clustering. (I) In contrast, a larger deletion of the C terminus leaving only 17 residues after the transmembrane domain abolished synaptic clustering. The C-terminal deletion still reached the neuron surface (see Figure S6). Scale bar, 10 μm.

YFP-LRRTM1 or YFP-LRRTM2, and then cultured in the presence of beads coated with anti-GFP antibodies. The antibody-coated beads induced robust clustering of YFP-LRRTMs at nonsynaptic sites (sites lacking VGLUT1 or VGAT) on the dendrites. Such artificial clustering of YFP-LRRTMs resulted in coclustering of the glutamatergic postsynaptic proteins NMDA receptor essential subunit NR1 (Figures 6A and 6B), PSD-95 family (Figures 6C and S7A), and SynGAP (Figure S7C). In contrast, artificial clustering of YFP-LRRTMs did not result in coclustering of the inhibitory postsynaptic protein gephyrin (Figures 6D and S7B). NR1

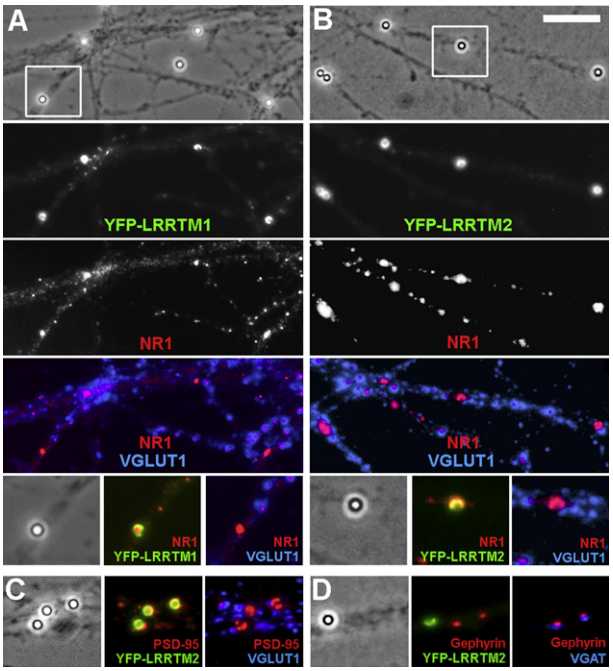

Figure 6. Clustering of LRRTMs Mediates Postsynaptic Differentiation

Neurons were transfected with YFP-LRRTM1 (A) or YFP-LRRTM2 (B–D) and the YFP fusion protein was artificially clustered using beads coated with antibodies to GFP. The 1 μm diameter beads are visible in the phase-contrast images. The anti-GFP beads effectively cluster the YFP fusion proteins. (A and B) Staining for the NMDA-type glutamate receptor essential subunit NR1 shows clustering of NR1 at bead induced clusters of YFP-LRRTMs, at nonsynaptic sites lacking VGLUT1. Additional NR1 clusters are observed at bona fide postsynaptic sites associated with VGLUT1. The boxed regions are shown magnified in the bottom panels. Scale bar, 10 μm. (C) PSD-95 family proteins also cluster at bead induced clusters of YFP-LRRTM, at nonsynaptic sites lacking VGLUT1. (D) The inhibitory postsynaptic marker gephyrin shows no clustering by bead clustered YFP-LRRTM.

immunofluorescence at bead-induced YFP-LRRTM2 clusters showed a 3.2-fold enrichment compared with the rest of the dendrite, and PSD-95 a 2.9-fold enrichment ($p < 0.005$, $n = 6–21$ cells), whereas gephyrin immunofluorescence was not enriched. These results suggest that LRRTMs may be involved in bidirectional signaling to recruit both postsynaptic and presynaptic components.

Localization of Endogenous LRRTM2 to Excitatory Synapses In Vivo

In order to assess the endogenous localization of LRRTM2, we generated rabbit polyclonal antibodies against peptide sequences in the C-terminal cytoplasmic tail of LRRTM2 (Figures 7A and S8). All four LRRTM mRNAs could be detected in cultured hippocampal neurons by RT-PCR (data not shown). However, with the LRRTM2 antibody only a weak signal was detected by western blot, and no endogenous immunofluorescence was detected in cultured neurons (data not shown), even though these antibodies could detect LRRTM2 immunofluorescence in YFP-LRRTM2-transfected cells (Figures S8D–S8G) and in brain sections (Figures 7C–7F). Thus, expression level of LRRTMs is low in cultured neurons.

To address the localization of LRRTM2 in the brain, we first performed synaptic fractionation from adult rat brain. Biochemical fractionation of whole-brain homogenate shows a strong enrichment of LRRTM2 in the PSD fraction, the detergent-resistant material following extraction of the synaptic plasma membrane fraction (Figure 7B). This PSD fraction is also highly enriched in PSD-95. We then examined localization of endogenous LRRTM2 in tissue sections using confocal microscopy. LRRTM2 is widely distributed in neuropil regions in discrete puncta throughout the brain. Consistent with the in situ hybridization data (Lauren et al., 2003), LRRTM2 protein was detected in cortex, thalamus, striatum, olfactory bulb, cerebellum, and all hippocampal subfields (Figures 7C and 7D and data not shown). Also consistent with LRRTM2 mRNA distribution, LRRTM2 protein is more abundant in deep than in superficial layers of neocortex. The protein further exhibits laminar-specific concentrations independent of mRNA distribution. In the CA1 region of hippocampus, LRRTM2 is more concentrated in stratum lacunosum moleculare than in radiatum or oriens (Figure 7C), and in CA3 LRRTM2 is most concentrated in stratum lucidum (Figure 7E). High expression of LRRTM2 mRNA by cerebellar granule cells corresponds to abundance of the protein at cerebellar glomeruli (Figure 7F). At these large discrete cerebellar glomerular rosettes and CA3 mossy fiber synapses, LRRTM2 immunofluorescence overlapped significantly with the general synaptic marker bassoon and the excitatory synaptic marker VGLUT1. Thus, both biochemical and immunofluorescence data support localization of LRRTM2 to glutamatergic postsynaptic sites in adult rodent brain.

Altered Distribution of VGLUT1 in *LRRTM1*$^{-/-}$ Mice

As shown above, all four LRRTMs have synaptogenic activity. LRRTM1 and LRRTM2 are most potent at inducing presynaptic differentiation, target to glutamate postsynaptic sites, and clustering of either on dendrites mediates postsynaptic differentiation. Expression patterns of the four LRRTMs overlap extensively in vivo (Lauren et al., 2003). Thus, it may require knockout of multiple family members to reveal a strong phenotype. We started an in vivo analysis of function here by generating genetically targeted mice lacking the family member isolated from the screen, LRRTM1 (Figures 8A–8C). *LRRTM1*$^{-/-}$ mice survived in the expected Mendelian ratios, were fertile, and displayed no overt phenotype. Brain morphology appeared grossly normal as assessed by cresyl violet stain (excepting that one of twelve *LRRTM1*$^{-/-}$ mice showed anomalous ventroculomegaly, data not shown). Cellular organization and synaptic distribution assessed by DAPI stain and bassoon immunofluorescence were indistinguishable from wild-type. Figure 8D shows images from the hippocampal formation, which, along with thalamus, normally expresses the highest levels of LRRTM1 (Lauren et al., 2003).

A quantitative immunofluorescence analysis revealed a synaptic defect in specific regions of the hippocampal formation in *LRRTM1*$^{-/-}$ young adult mice (Figures 8E–8G). The measures revealed a selective increase in the size of VGLUT1 puncta in CA1 stratum radiatum and stratum oriens, but no change in CA1 stratum lacunosum moleculare or CA3 stratum lucidum. Puncta density and intensity did not differ (Figure S9). The finding that

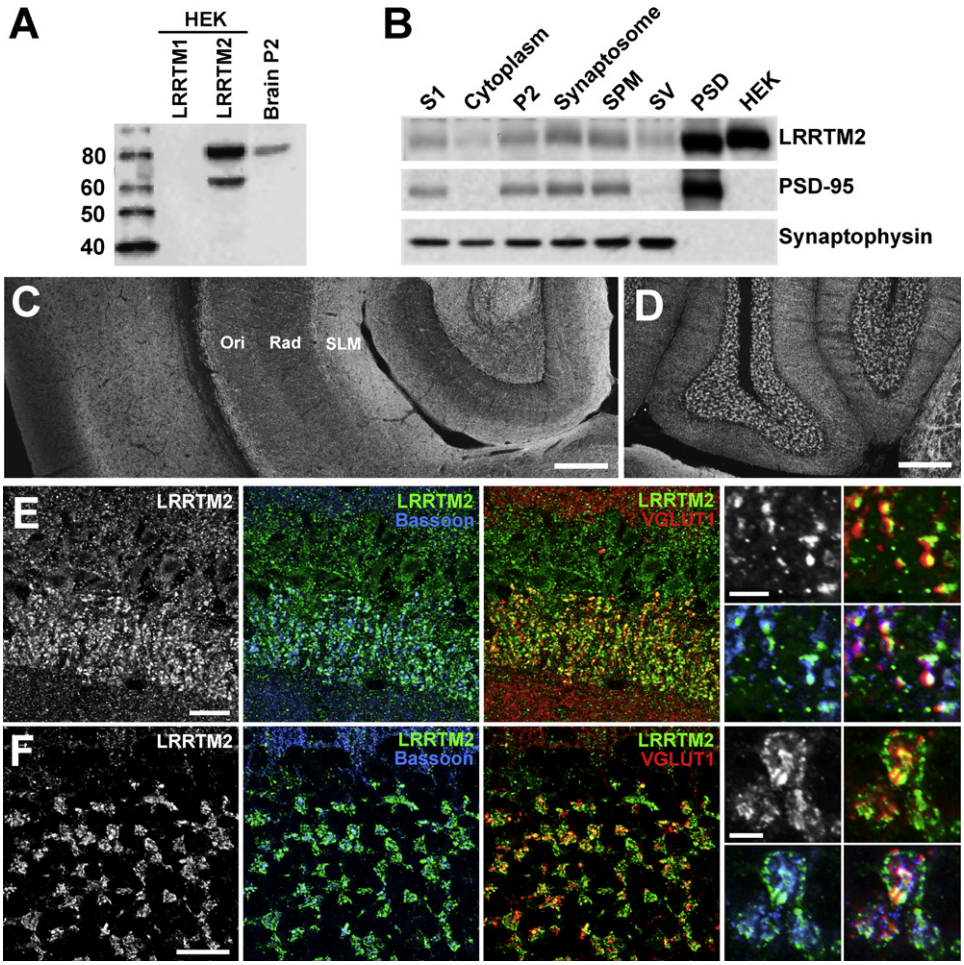

Figure 7. Localization of LRRTM2 to Excitatory Synapses In Vivo

(A) An antibody against LRRTM2 was generated. The blot shows recognition of an ~80 kDa protein in brain P2 lysate and in HEK cells transfected for recombinant LRRTM2 but not LRRTM1.

(B) Synaptic fractionation of adult rat brain homogenate. The ~80 kDa band corresponding to LRRTM2 is abundant in the PSD fraction along with PSD-95. LRRTM2 is detected in the P2, synaptosome, and synaptic plasma membrane (SPM) fractions but less so in the cytoplasm and synaptic vesicle (SV) fractions.

(C–F) Confocal analysis of LRRTM2 immunofluorescence in mouse brain sections. (C) LRRTM2 is widely detected in synaptic neuropil regions throughout the cortex and hippocampal formation. LRRTM2 exhibits a laminar-selective distribution; for example, in the CA1 region, LRRTM2 is present at higher levels in stratum lacunosum moleculare (SLM) than in radiatum (Rad) or oriens (Ori). (D) LRRTM2 is detected in the granule cell layer and molecular layer of the cerebellum. (C and D) Scale bar, 200 μm. (E) In hippocampus, LRRTM2 is particularly prominent in CA3 mossy fibers synapses shown here. Colocalization with the general synaptic marker bassoon and the excitatory synaptic marker VGLUT1 is shown. Enlarged regions are shown in the same color channels as the main panels (upper left LRRTM2 grayscale; lower left LRRTM2 green with bassoon blue; upper right LRRTM2 green with VGLUT1 red; lower right triple-channel overlay). (F) LRRTM2 also colocalized with bassoon and VGLUT1 in cerebellar glomerular synapses. (E and F) Scale bar, 20 μm in main panels, 5 μm in enlarged regions.

immunofluorescence for the active zone protein bassoon was not significantly different, in puncta size, density, or intensity, in these same double-labeled samples serves as an internal procedural control and indicates a selective change in the glutamatergic vesicle localized VGLUT1. The increased size of fluorescence puncta for VGLUT1 may indicate a dispersal of synaptic vesicles. A similar increase in size of fluorescence puncta for synaptophysin in neurons lacking β-catenin corresponded to a dispersal of synaptic vesicles and reduction in reserved pool vesicles (Bamji et al., 2003). LRRTM2 is highly coexpressed in CA1 with LRRTM1, and both LRRTM2 and LRRTM4 are coexpressed in CA3 (Lauren et al., 2003). Specifically, the region of CA1 with the highest level of LRRTM2 immunoreactivity, lacunosum moleculare, did not show any alteration in VGLUT1 distribution in the *LRRTM1*$^{-/-}$ mice, synaptic defects were only seen in radiatum and oriens, which have relatively lower levels of LRRTM2 (See Figure 7C for LRRTM2 immunoreactivity in CA1 regions).

Prevalence of Novel and LRR Proteins from the Unbiased Screen

While these results validate LRRTMs as synaptogenic proteins, we sought to determine the extent to which known synaptogenic proteins plus LRRTMs explain the spectrum of brain synaptogenic activity. A total of 521 pools of cDNA expression plasmids,

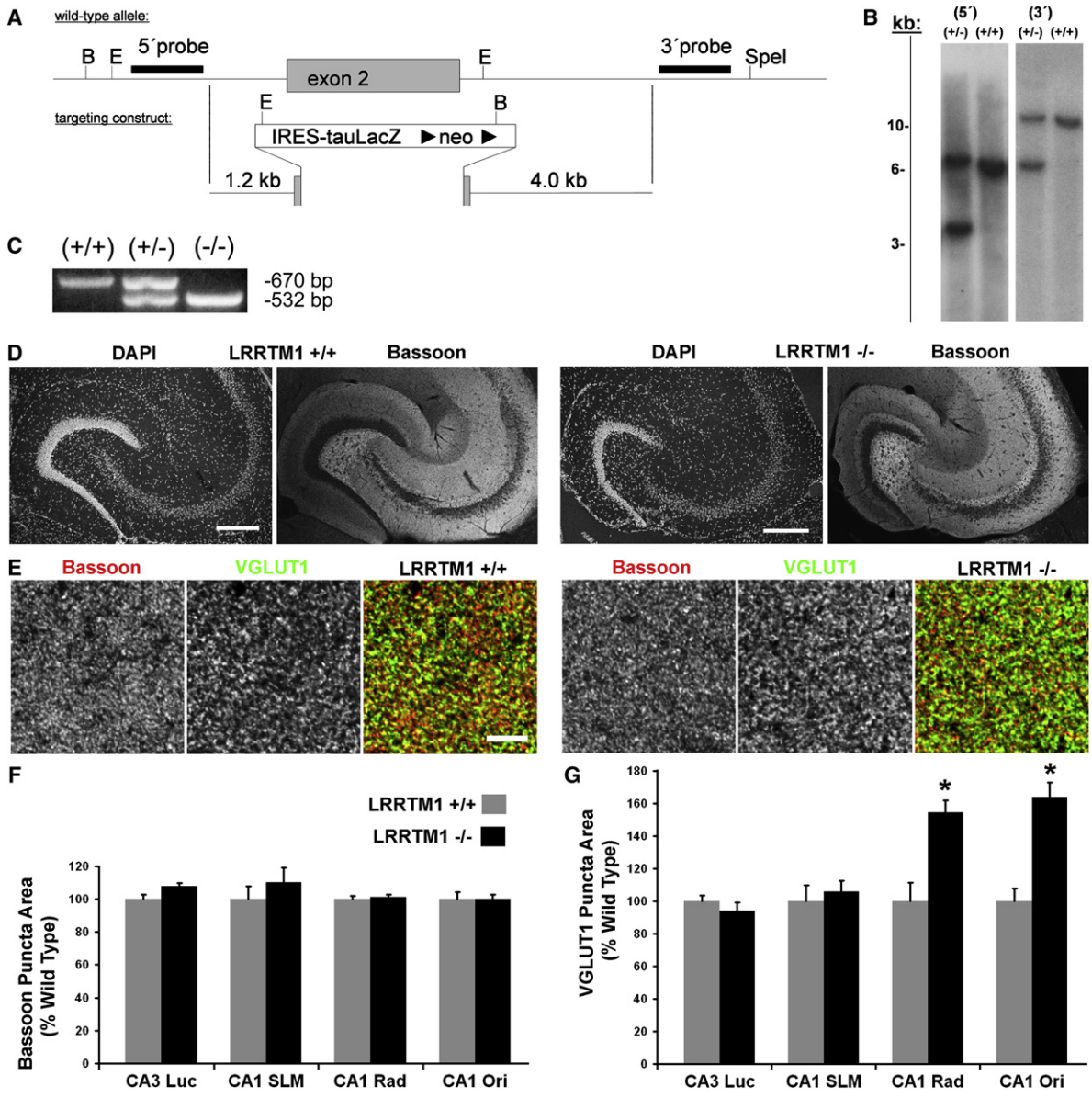

Figure 8. Normal Brain Morphology but Altered VGLUT1 Immunofluorescence in *LRRTM1*$^{-/-}$ Mice

(A) Targeting strategy for *Lrrtm1* locus. Part of the wild-type *Lrrtm1* locus as well as the elements of the replacing cassette are shown. The locations of the restriction enzyme cleavage sites used in the Southern blotting analysis are indicated: B, BamHI; E, EcoRI; IRES, internal ribosome entry site.

(B) Southern blotting results with a correctly targeted ES cell clone (+/−) and with a wild-type (+/+) ES cell clone are shown. Fragment lengths expected are 6 kb for wild-type and 3.6 kb for a correctly targeted allele with the 5′ probe (EcoRI digest), and 10.5 kb for wild-type and 5.4 kb for a correctly targeted allele with the 3′ probe (BamHI and SpeI digest).

(C) Genotyping results for wild-type (+/+) mouse and mice heterozygous (+/−) or homozygous (−/−) for *Lrrtm1* deletion.

(D) No differences were detected in overall cellular or synaptic distribution in the *LRRTM1*$^{-/-}$ mouse brain compared with wild-type. DAPI stain for nuclei shows normal cellular organization in the hippocampal formation. Immunofluorescence patterns for the presynaptic active zone protein bassoon are indistinguishable between *LRRTM*$^{-/-}$ and wild-type hippocampus. Scale bar, 200 μm.

(E–G) Quantitative analysis of immunofluorescence in the hippocampal formation at 4–5 weeks. (E) Sample confocal images, here from CA1 stratum radiatum. Scale bar, 10 μm. (F) There was no difference in bassoon immunopositive puncta area between *LRRTM1*$^{-/-}$ and wild-type in any region measured. Measures were made from the same multichannel images as for panel (G). (G) Puncta area for the vesicle-associated protein VGLUT1 was selectively increased in CA1 stratum radiatum (Rad) and oriens (Ori) (t test $p < 0.01$, duplicate experiments of two *LRRTM1*$^{-/-}$ and three wild-type mice), but unchanged in *LRRTM1*$^{-/-}$ relative to wild-type mice in CA1 stratum lacunosum moleculare (SLM) and CA3 stratum lucidum (Luc). Mean values for VGLUT1 puncta area in wild-type mice were 1.01 μm^2 CA3 Luc, 0.50 μm^2 CA1 SLM, 0.49 μm^2 CA1 Rad, 0.50 μm^2 CA1 Ori.

Panels (A)–(C) are reproduced from a doctoral dissertation (Lauren, 2007). All error bars are SEM.

Table 1. Results from COS Cell and Neuron Coculture Screen of Expression Libraries

Size Range	# cDNAs Screened[a]	Positives[b]	Extracellular Domains	Conserved C Terminus
1–2 kb	22,000	none		
2–3 kb	52,050	NGL-3/LRRC4B	LRR, Ig	-ETQI
		PB243		
		PB270		
3–4 kb	22,250	LRRTM1	LRR	-ECEV
		PC151		
4–5 kb	26,750	neuroligin-2 (3X)	AChE	-TTRV

[a] Clones were screened in pools of ~200–250 clones each, in 521 pools.
[b] PB/Cxxx are positive pools that contain novel synaptogenic proteins.

representing 123,050 independent clones, were tested in the coculture assay. Eight pools scored positive for ability to cluster synapsin in contacting axons, in the absence of postsynaptic markers (Table 1). Four pools contained known synaptogenic proteins, neuroligin-2 (Figure S10; Scheiffele et al., 2000) or NGL-3/LRRC4B (Figure S11; Kim et al., 2006). Thus, two of the four previously identified synaptogenic families (neuroligins, EphBs, SynCAMs, and NGLs) were reisolated in this screen. The additional positive pools do not contain known synaptogenic proteins or LRRTMs, as assessed by PCR, and presumably include novel clones. A majority of the synaptogenic proteins scoring positive in this unbiased screen were previously unidentified using other approaches. Of the three synaptogenic protein families identified here, all contain C-terminal PDZ domain binding sequences conserved among all family members, and two contain extracellular leucine-rich repeats (Table 1).

We next tested whether the results of this unbiased screen could be used to further predict additional synaptogenic proteins. New candidates were chosen based on primary sequence by the presence of predicted extracellular LRR domains, a single transmembrane domain, and a C-terminal sequence bearing a consensus PDZ domain binding site and/or highly conserved among family members and species. One of the six additional candidates chosen, Slitrk2, tested positive in the coculture assay for ability to induce clusters of synapsin in contacting hippocampal axons (Figure S12).

DISCUSSION

We performed here a function-based discovery screen in a mammalian system for proteins that can instruct presynaptic differentiation. In addition to isolating positive pools containing neuroligin-2 and NGL-3 cDNAs, we identified LRRTM1 as synaptogenic. We show that LRRTM1 instructs excitatory presynaptic differentiation in contacting axons, mediates excitatory postsynaptic differentiation in dendrites, localizes to excitatory postsynaptic sites, and is required for normal VGLUT1 distribution in vivo. These results provide a cellular basis for the linkage of LRRTM1 to handedness and schizophrenia (Francks et al., 2007). Results from this unbiased screen suggest that only about half of mammalian synaptogenic proteins have been found by other approaches and reveal a prevalence of LRR proteins as synaptic organizers. Thus, the first major contribution of this work is to develop a function-based unbiased screen to identify novel mammalian synaptic proteins. The second major contribution is to characterize the synapse-organizing activity of LRRTM proteins.

When this project was initiated, there was considerable uncertainty as to whether neuroligin was unique as a synaptogenic factor or whether it was one of several such proteins. While an unbiased search for such activity was likely to provide the most convincing resolution of this issue, it remained unclear if a broad synaptogenesis screen was feasible. After screening over 10^5 cDNAs, we can conclude that multiple synaptogenic protein families exist and that our knowledge of synaptogenic factors does not yet include a full catalog of relevant cell surface signals. The unbiased screen as performed here isolated only the most potent synaptogenic factors. We identified neuroligin-3 by PCR in a pool that was scored as negative for synaptogenic activity in the screen. Yet neuroligin-3 is able to induce presynaptic differentiation in coculture (Chih et al., 2004). Thus, smaller pool sizes may be needed to identify synaptogenic factors less potent than neuroligin-2, NGL-3, and LRRTM1.

The LRRTM protein family was initially identified while looking for proteins sharing sequence similarity to the Slit family of axon guidance molecules (Lauren et al., 2003). The LRRTM protein family is restricted to vertebrates and consists of four members in mammals. All four family members are expressed in mouse brain from P0 or earlier through adult (Lauren et al., 2003). Each LRRTM family member displays the ability to instruct excitatory presynaptic differentiation.

LRRTM3 displayed the weakest activity among the LRRTMs despite good apparent cell surface localization. Since LRRTM3 expression is low in hippocampus and higher in cortex (Lauren et al., 2003), we also tested LRRTM3-CFP and LRRTM2-CFP in a coculture assay using neocortical neurons. LRRTM3 was much less effective as a synaptogenic factor using both neuronal types (data not shown). Additionally, LRRTM3-CFP was often concentrated in the COS cells along the length of contacting hippocampal axons in a nonpunctate distribution (data not shown), suggesting the presence of a binding partner along the length of axons and not specifically at presynaptic sites. These observations suggest that the function of LRRTM3 may be significantly different from that of the other family members. LRRTM3 was recently identified in an siRNA screen to promote processing of amyloid precursor protein by BACE1 to increase Aβ secretion, a function not shared by the other family members (Majercak et al., 2006).

LRRTM2 localized specifically to glutamatergic and not GABAergic synapses in hippocampal culture (Figure 5C), and the LRRTM2 LRR domain on beads could instruct glutamatergic but not GABAergic presynaptic differentiation (Figure 4). Thus it is not clear why LRRTM2 on COS cells was able to instruct GABAergic as well as glutamatergic presynaptic differentiation (Figures S3D and S3F). We suspect that the local concentration of LRRTM2 available for presentation to axons may reach higher levels on COS cells than on beads or at postsynaptic sites, allowing for low-affinity interactions with GABAergic axons. Similarly, neuroligin-2 instructs both excitatory and inhibitory presynaptic

differentiation in the coculture assay, yet neuroligin-2 is exclusively localized to inhibitory synapses under normal conditions (Chih et al., 2005; Graf et al., 2004; Varoqueaux et al., 2004). The distribution of neuroligin-2 can be shifted to excitatory synapses upon overexpression of PSD-95, leading to the idea that the ratio of postsynaptic organizing molecules may control the ratio of excitatory to inhibitory inputs (Levinson et al., 2005). Perhaps like neuroligins, LRRTM2 may function at both synapse types under some conditions.

Our immunohistochemical localization of LRRTM2 in brain was consistent with the in situ hybridization pattern (Lauren et al., 2003), widespread expression particularly prominent in cerebellar granule cells, the deeper layers of neocortex, and all major cell layers of the hippocampus. The laminar distribution of LRRTM2 within the hippocampus (Figure 7C) suggests a selective targeting of the protein. NGL-1, an LRR domain containing synaptic adhesion protein related to NGL-3 isolated in our screen, is also selectively concentrated in CA1 dendrites in stratum lacunosum moleculare opposite temporoammonic inputs from the entorhinal cortex (Nishimura-Akiyoshi et al., 2007). NGL-1 redistributed equally to radiatum and oriens upon targeted deletion of its axonal ligand netrin-G1. The laminar-selective distribution of LRRTM2 may also be related to expression of an axonal ligand by specific inputs. The LRRTM2 LRR-AP protein did not bind cells expressing LRRTM2-CFP under conditions where positive control neurexin-AP bound cells expressing neuroligin-2-CFP (data not shown), suggesting the absence of LRRTM homophilic binding.

The combined results of our screen suggest that LRR proteins may be prevalent as synaptic cell adhesion and organizing proteins, with two of the three proteins isolated here containing LRR domains. Screening of an additional six LRR protein candidates chosen only by primary sequence further identified Slitrk2 as synaptogenic. The Slitrk family was recently identified based on homology to Slit secreted axon guidance molecules and Trk neurotrophin receptors (Aruga and Mikoshiba, 2003). Little is reported about cellular function other than ability to alter neurite outgrowth, but mutations in Slitrk1 are associated with Tourette's Syndrome (Abelson et al., 2005), and targeted deletion of Slitrk1 in mice results in behavioral abnormalities (Katayama et al., 2008). LRRTMs and Slitrks were not included in a set of 160 candidates tested recently by RNAi for a role in synapse development; LRRC4C and LRRN6A were tested but found to have no effect in this study, which identified a role for cadherins and semaphorins in synapse development (Paradis et al., 2007). Mammalian LRR transmembrane proteins previously shown to have a synaptic function are NGLs and SALMs (Ko and Kim, 2007). NGL-1 is reported to be important for axon outgrowth (Lin et al., 2003), and subsequently NGLs were found to bind PSD-95 (Kim et al., 2006). Like LRRTMs, NGL-2 can promote excitatory presynaptic differentiation using both bead and cellular coculture assays (Kim et al., 2006). NGL-1 and NGL-2 bind netrin-G1 and netrin-G2, respectively. However, direct aggregation of netrin-G2 on axons does not mediate presynaptic differentiation, nor does netrin-G2 induce postsynaptic differentiation in coculture (Kim et al., 2006). Thus, like LRRTMs, the axonal binding partner that mediates the synaptogenic activity of NGLs remains to be fully identified. SALMs also bind PSD-95, and artificial clustering of SALM2 on dendrites directly mediates postsynaptic differentiation, but SALMs do not instruct presynaptic differentiation in coculture assays (Ko et al., 2006; Wang et al., 2006). A recent expression screen in *Drosophila* also identified several other LRR proteins as important in synaptic target selection (Kurusu et al., 2008). Determining how these multiple synaptic LRR proteins function cooperatively, and identifying their binding partners, whether unique or common, is emerging as a major challenge.

A specific component of this challenge will be to define the precise role of LRRTM1-4 at synapses. The ability of a protein to induce presynaptic specializations in the coculture assay does not necessarily imply that its endogenous function is in synapse initiation. Given the highly interconnected network of proteins at presynaptic specializations in axons, any protein that tightly binds to a transmembrane component of such complexes could potentially instruct presynaptic differentiation. Therefore, the coculture screen could yield proteins that are involved in later stages of synaptic maturation, perhaps in recruiting specific components that regulate selective synaptic parameters. In some respects, neuroligins fit this description. While neuroligins are potent synaptogenic factors in the coculture assay, and neuroligin-1, -2, -3 triple-knockout mice die due to defects in synaptic function, loss of all neuroligins does not result in an obvious effect on overall synapse morphology (Varoqueaux et al., 2006). Furthermore, like the phenotype of *LRRTM1*$^{-/-}$ mice reported here, the phenotype of individual neuroligin knockouts is subtle. The only defect reported for the neuroligin-1 null mouse is a reduced NMDA to AMPA ratio at CA1 synapses in acutely prepared slices (Chubykin et al., 2007; Varoqueaux et al., 2006). Similarly, triple mutation of EphB1 plus EphB2 plus EphB3 is required to observe any reduction in spine density in CA1 or neocortex, since single or double EphB mutants exhibit no spine phenotype (Henkemeyer et al., 2003; Kayser et al., 2006).

In addition to this clear evidence for redundancy among members of each family of synaptogenic proteins, many synaptic phenotypes tend to be apparent exclusively in vivo. For example, dissociated cortical cultures from the neuroligin triple knockouts show normal excitatory transmission and synapse density and composition (Varoqueaux et al., 2006). These observations, coupled with the apparent low level of expression of LRRTMs in hippocampal neurons in dissociated culture suggest that the function of these synaptic organizing molecules may be assessed accurately only by in vivo studies. The altered distribution of VGLUT1 but not bassoon in specific hippocampal subfields with in vivo deletion of LRRTM1 as reported here supports a role in selective recruitment of synaptic components. Further ultrastructural, electrophysiological and behavioral analyses will be required to fully characterize the effect of deletion of LRRTM1.

Recently, LRRTM1 was shown to be linked via paternal transmission with handedness and schizophrenia (Francks et al., 2007). This finding is intriguing given our results indicating a synaptic function for LRRTM1. Schizophrenia is likely to be etiologically complex, with many genetic, epigenetic, and environmental influences. Nonetheless, the identification of genetic alterations associated with complex disorders even in rare cases

can lead to the development of animal models, such as the neuroligin-3 R451C knockin, neuroligin-4 knockout, and neuroligin-2 transgenic mouse models of autism (Hines et al., 2008; Jamain et al., 2008; Tabuchi et al., 2007). Thus, it is possible that our molecular and cellular level studies on LRRTM1 may lead to new directions of research on schizophrenia.

EXPERIMENTAL PROCEDURES

More detailed experimental procedures are described in the Supplemental Data.

Generation of the Full-Length, Size-Selected Expression Libraries

Rat brains were dissected at P11, and the cerebellum and brainstem were removed. Total RNA was prepared using the method of Carninci and Hayashizaki (1999), and mRNA was further purified using the Ambion Poly(A)Purist MAG kit. For purification of full-length cDNA, the biotinylated cap-trapper protocol was implemented (Carninci et al., 1996). The first-strand synthesis products are oxidized and 5′-cap and 3′-hydroxyl groups are biotinylated. Limited RNase I digestion cleaves unhybridized RNA, thus eliminating the 5′ biotin tag on first-strand products that are not full length. The remaining biotinylated mRNA:cDNA hybrids are purified using streptavidin magnetic beads, and single-stranded full-length cDNA is released following sodium hydroxide hydrolysis of the mRNA strand. For second-strand synthesis, we developed a modification of the single-stranded linker ligation method (SSLLM) to attach a linker with a BamH I site to the cDNA (Shibata et al., 2001). Full-length cDNA was digested and size-fractionated using a 1% low-melt agarose gel before ligation into the pcDNA3 vector.

Cell Culture

Cultures of hippocampal neurons were prepared from E18 rat embryos according to previously described protocols (Goslin et al., 1998; Kaech and Banker, 2006). COS-7 and HEK293T cells were cultured in DMEM-H supplemented with 10% fetal bovine serum. Cocultures of COS or HEK293T cells and neurons were performed essentially as described (Graf et al., 2004). For the expression screen, COS cells were transfected in 12-well plates with 500 ng of plasmid from each expression pool. Transfected COS cells were harvested by trypsinization after 7 or 24 hr, seeded onto neuron coverslips pregrown for 8–9 DIV, and fixed for screening 20 hr later.

Immunocytochemistry and Culture Imaging

For screening, cocultures were fixed for 12 min with 4% paraformaldehyde and 4% sucrose in PBS (pH 7.4) followed by permeabilization with PBST (PBS + 0.1% Triton X-100). An initial blocking step was performed with PBS-BSA/NGS (3% BSA, 5% normal goat serum) for 30 min at 37°C. Cocultures were incubated overnight in anti-synapsin I (1:2000; Millipore), anti-PSD-95 family (IgG2a; 1:500; clone 6G6-1C9; Affinity Bioreagents; recognizes PSD-95, PSD-93, SAP102 and SAP97), and anti-gephyrin (IgG1; 1:1000; mAb7a; Synaptic Systems) in PBS-BSA/NGS. After washing with PBS, cocultures were incubated in Alexa-488-conjugated goat anti-rabbit (1:500; Molecular Probes) and Texas Red-conjugated goat anti-mouse (1:500; Invitrogen) was used to detect gephyrin and PSD-95 in the same channel. After washing in PBS, the coverslips were incubated with 200 ng/ml DAPI in PBS for 20 min, washed, and mounted in elvanol (Tris-HCl, glycerol, and polyvinyl alcohol, with 2% 1,4-diazabicyclo[2,2,2]octane). Primary antibodies used for other experiments were rabbit anti-VGAT (1:2000; Synaptic Systems), anti-SynGAP (1:2000; Affinity BioReagents), mouse anti-Tau-1, clone PC1C6 (IgG2A; 1:2000; Millipore; recognizes dephosphorylated tau), anti-bassoon (IgG2A; 1:1000; Stressgen), anti-synaptophysin (IgG1; 1:1000; BD Biosciences), anti-NMDAR1, clone 54.1 (IgG2a; 1:1000; BD Biosciences), guinea pig anti-VGLUT1 (1:4000; Millipore), and chicken anti-MAP2 (IgY; 1:8000; Abcam).

Images were acquired on a Zeiss Axioplan2 microscope with a 63× 1.4 numerical aperture oil objective and Photometrics Sensys cooled CCD camera using Metamorph imaging software (Molecular Devices) and customized filter sets. Controls lacking specific antibodies confirmed no detectable bleed-through between channels AMCA, CFP, YFP or Alexa 488 (imaged through a YFP filter set), Alexa 568, and Alexa 647. For quantitation, sets of cells were cocultured and stained simultaneously and imaged with identical settings. All imaging and analysis were done blind.

Electrophysiology

Whole-cell patch-clamp recordings were made at room temperature in Mg^{2+}-free extracellular solution (168 mM NaCl, 2.4 mM KCl, 10 mM HEPES, 10 mM D-glucose, 1.3 mM $CaCl_2$, 20 μM glycine, pH 7.4, osmolality adjusted with sucrose). HEK293T cells were voltage clamped at −60 mV, spontaneous currents recorded, and then mEPSC-like events recorded in the presence of 1 μM TTX. All activity was blocked with 100 μM APV. NMDA receptor-mediated spontaneous events and mEPSC-like events were both measured with the Axograph software using an optimally scaled sliding template (Clements and Bekkers, 1997) and criteria of three times the SD. The measures likely underestimate frequency for the LRRTM2 group without TTX.

Bead Clustering Experiments

For clustering of YFP-LRRTMs, we used a protocol that had been previously used to cluster YFP-neuroligins (Graf et al., 2004). For the presynaptic induction assay, 1 μm NeutrAvidin-labeled Fluospheres were mixed by constant inversion at room temperature in HBS + BSA (10 mM HEPES, pH 7.3, 145 mM NaCl, 5 mM KCl, 2 mM $MgCl_2$, 2 mM $CaCl_2$, 100 μg/ml BSA). The beads were incubated with biotinylated anti-myc tag (IgG1; Millipore 16-170; 17 μg per 10 μl beads), washed, then incubated with 60 μg of either the soluble control AP protein or the LRRTM2 LRR-AP protein for 2 hr in HBS + BSA. Coated beads were resuspended in conditioned media and applied to 8 DIV hippocampal neurons. Neurons were cultured in the presence of coated beads for 20–24 hr, and fixed the following day for immunocytochemistry.

Generation and Analysis of *LRRTM1*$^{-/-}$ Mice

The entire mouse Lrrtm1 open reading frame (ORF) is encoded by a single exon. Thus, to generate LRRTM1 knockout mice this exon was chosen for gene targeting. The plasmid used in the construction of the targeting construct was obtained from Dr. Peter Mombaerts (Rodriguez et al., 1999). The ES cell clones were analyzed by Southern blotting for the evidence of homologous recombination (Figure 8).

Identical conditions were used for immunostaining as well as capture and analysis of confocal images for each condition. Each experiment was performed blind and in duplicate. Mice were perfused at 4–5 weeks with 2% paraformaldehyde in PBS, brains postfixed and cryoprotected in 30% (w/v) sucrose in PBS. Cryostat sections (20 μm) were incubated in blocking solution containing 0.1 M PBS, 5% normal goat serum, 5% BSA, and 0.25% Triton X-100, then overnight at 4°C with anti-Bassoon (1:1000, Stressgen) and anti-VGLUT1 (1:300; NeuroMab N28/9) in blocking solution, then with Alexa dye conjugated secondary antibodies. Confocal images (0.37 μm optical section at 5 μm below the tissue surface) were captured sequentially on a Fluoview FV500 confocal system from five separate fields per anatomical region per animal. Three wild-type and two knockout animals were used for analysis. Images were analyzed using MetaMorph. A single threshold was set for each staining condition to capture clusters that were clearly distinguishable and to minimize merged clusters. The number, size, and intensity of the puncta were measured. Data from wild-type and knockout images were compared using Student's t tests.

SUPPLEMENTAL DATA

The Supplemental Data include Supplemental Experimental Procedures and 12 figures and can be found with this article online at http://www.neuron.org/supplemental/S0896-6273(09)00084-1.

ACKNOWLEDGMENTS

We thank Xiling Zhou and Huaiyang Wu for consistent excellence in preparation of hippocampal neuron cultures. Fernanda Laezza, Vanessa Santiago, and Ann Chow provided assistance with preparation of RNA, cDNA pools, and PLAP fusion proteins. Katherine Walzak and Susan Hand provided

assistance with coculture assays and immunofluorescence for revision experiments. We thank Dr. Robert Holt and team at the Michael Smith Genome Sciences Centre for arraying the cDNA subpool and preparing DNA in 384-well format. We also thank Drs. Joshua Sanes for input in the early stages of this work and Tabrez Siddiqui for helpful comments on the manuscript. This work was supported by CIHR MOP-84241, NIH MH070860, and CRC and MSFHR salary awards to A.M.C., NIH NS03220 and NS39962 to S.M.S., CIHR and MSFHR fellowships to F.A.D., and JSPS fellowship to H.T.

Accepted: January 8, 2009
Published: March 11, 2009

REFERENCES

Abelson, J.F., Kwan, K.Y., O'Roak, B.J., Baek, D.Y., Stillman, A.A., Morgan, T.M., Mathews, C.A., Pauls, D.L., Rasin, M.R., Gunel, M., et al. (2005). Sequence variants in SLITRK1 are associated with Tourette's syndrome. Science *310*, 317–320.

Ackley, B.D., and Jin, Y. (2004). Genetic analysis of synaptic target recognition and assembly. Trends Neurosci. *27*, 540–547.

Aoto, J., Ting, P., Maghsoodi, B., Xu, N., Henkemeyer, M., and Chen, L. (2007). Postsynaptic ephrinB3 promotes shaft glutamatergic synapse formation. J. Neurosci. *27*, 7508–7519.

Aruga, J., and Mikoshiba, K. (2003). Identification and characterization of Slitrk, a novel neuronal transmembrane protein family controlling neurite outgrowth. Mol. Cell. Neurosci. *24*, 117–129.

Bamji, S.X., Shimazu, K., Kimes, N., Huelsken, J., Birchmeier, W., Lu, B., and Reichardt, L.F. (2003). Role of beta-catenin in synaptic vesicle localization and presynaptic assembly. Neuron *40*, 719–731.

Biederer, T., and Scheiffele, P. (2007). Mixed-culture assays for analyzing neuronal synapse formation. Nat. Protocols *2*, 670–676.

Biederer, T., Sara, Y., Mozhayeva, M., Atasoy, D., Liu, X., Kavalali, E.T., and Sudhof, T.C. (2002). SynCAM, a synaptic adhesion molecule that drives synapse assembly. Science *297*, 1525–1531.

Carninci, P., and Hayashizaki, Y. (1999). High-efficiency full-length cDNA cloning. Methods Enzymol. *303*, 19–44.

Carninci, P., Kvam, C., Kitamura, A., Ohsumi, T., Okazaki, Y., Itoh, M., Kamiya, M., Shibata, K., Sasaki, N., Izawa, M., et al. (1996). High-efficiency full-length cDNA cloning by biotinylated CAP trapper. Genomics *37*, 327–336.

Chih, B., Afridi, S.K., Clark, L., and Scheiffele, P. (2004). Disorder-associated mutations lead to functional inactivation of neuroligins. Hum. Mol. Genet. *13*, 1471–1477.

Chih, B., Engelman, H., and Scheiffele, P. (2005). Control of excitatory and inhibitory synapse formation by neuroligins. Science *307*, 1324–1328.

Chubykin, A.A., Atasoy, D., Etherton, M.R., Brose, N., Kavalali, E.T., Gibson, J.R., and Sudhof, T.C. (2007). Activity-dependent validation of excitatory versus inhibitory synapses by neuroligin-1 versus neuroligin-2. Neuron *54*, 919–931.

Clements, J.D., and Bekkers, J.M. (1997). Detection of spontaneous synaptic events with an optimally scaled template. Biophys. J. *73*, 220–229.

Craig, A.M., and Kang, Y. (2007). Neurexin-neuroligin signaling in synapse development. Curr. Opin. Neurobiol. *17*, 43–52.

Craig, A.M., Graf, E.R., and Linhoff, M.W. (2006). How to build a central synapse: clues from cell culture. Trends Neurosci. *29*, 8–20.

Dalva, M.B., McClelland, A.C., and Kayser, M.S. (2007). Cell adhesion molecules: signalling functions at the synapse. Nat. Rev. Neurosci. *8*, 206–220.

Fournier, A.E., GrandPre, T., and Strittmatter, S.M. (2001). Identification of a receptor mediating Nogo-66 inhibition of axonal regeneration. Nature *409*, 341–346.

Francks, C., Maegawa, S., Lauren, J., Abrahams, B.S., Velayos-Baeza, A., Medland, S.E., Colella, S., Groszer, M., McAuley, E.Z., Caffrey, T.M., et al. (2007). LRRTM1 on chromosome 2p12 is a maternally suppressed gene that is associated paternally with handedness and schizophrenia. Mol. Psychiatry *12*, 1129–1139, 1057.

Fu, Z., Washbourne, P., Ortinski, P., and Vicini, S. (2003). Functional excitatory synapses in HEK293 cells expressing neuroligin and glutamate receptors. J. Neurophysiol. *90*, 3950–3957.

Goslin, K., Asmussen, H., and Banker, G. (1998). Rat hippocampal neurons in low-density culture. In Culturing Nerve Cells, G. Banker and K. Goslin, eds. (Cambridge: MIT Press), pp. 339–370.

Graf, E.R., Zhang, X., Jin, S.X., Linhoff, M.W., and Craig, A.M. (2004). Neurexins induce differentiation of GABA and glutamate postsynaptic specializations via neuroligins. Cell *119*, 1013–1026.

Henderson, J.T., Georgiou, J., Jia, Z., Robertson, J., Elowe, S., Roder, J.C., and Pawson, T. (2001). The receptor tyrosine kinase EphB2 regulates NMDA-dependent synaptic function. Neuron *32*, 1041–1056.

Henkemeyer, M., Itkis, O.S., Ngo, M., Hickmott, P.W., and Ethell, I.M. (2003). Multiple EphB receptor tyrosine kinases shape dendritic spines in the hippocampus. J. Cell Biol. *163*, 1313–1326.

Hines, R.M., Wu, L., Hines, D.J., Steenland, H., Mansour, S., Dahlhaus, R., Singaraja, R.R., Cao, X., Sammler, E., Hormuzdi, S.G., et al. (2008). Synaptic imbalance, stereotypies, and impaired social interactions in mice with altered neuroligin 2 expression. J. Neurosci. *28*, 6055–6067.

Jamain, S., Radyushkin, K., Hammerschmidt, K., Granon, S., Boretius, S., Varoqueaux, F., Ramanantsoa, N., Gallego, J., Ronnenberg, A., Winter, D., et al. (2008). Reduced social interaction and ultrasonic communication in a mouse model of monogenic heritable autism. Proc. Natl. Acad. Sci. USA *105*, 1710–1715.

Kaech, S., and Banker, G. (2006). Culturing hippocampal neurons. Nat. Protocols *1*, 2406–2415.

Katayama, K., Yamada, K., Ornthanalai, V.G., Inoue, T., Ota, M., Murphy, N.P., and Aruga, J. (2008). Slitrk1-deficient mice display elevated anxiety-like behavior and noradrenergic abnormalities. Mol. Psychiatry, in press. Published online September 16, 2008. 10.1038/mp.2008.97.

Kayser, M.S., McClelland, A.C., Hughes, E.G., and Dalva, M.B. (2006). Intracellular and trans-synaptic regulation of glutamatergic synaptogenesis by EphB receptors. J. Neurosci. *26*, 12152–12164.

Kim, S., Burette, A., Chung, H.S., Kwon, S.K., Woo, J., Lee, H.W., Kim, K., Kim, H., Weinberg, R.J., and Kim, E. (2006). NGL family PSD-95-interacting adhesion molecules regulate excitatory synapse formation. Nat. Neurosci. *9*, 1294–1301.

Ko, J., and Kim, E. (2007). Leucine-rich repeat proteins of synapses. J. Neurosci. Res. *85*, 2824–2832.

Ko, J., Kim, S., Chung, H.S., Kim, K., Han, K., Kim, H., Jun, H., Kaang, B.K., and Kim, E. (2006). SALM synaptic cell adhesion-like molecules regulate the differentiation of excitatory synapses. Neuron *50*, 233–245.

Krueger, S.R., Kolar, A., and Fitzsimonds, R.M. (2003). The presynaptic release apparatus is functional in the absence of dendritic contact and highly mobile within isolated axons. Neuron *40*, 945–957.

Kuja-Panula, J., Kiiltomaki, M., Yamashiro, T., Rouhiainen, A., and Rauvala, H. (2003). AMIGO, a transmembrane protein implicated in axon tract development, defines a novel protein family with leucine-rich repeats. J. Cell Biol. *160*, 963–973.

Kurusu, M., Cording, A., Taniguchi, M., Menon, K., Suzuki, E., and Zinn, K. (2008). A screen of cell-surface molecules identifies leucine-rich repeat proteins as key mediators of synaptic target selection. Neuron *59*, 972–985.

Lauren, J. (2007). Characterization of LRRTM and NGR Gene Families: Expression and Functions (Helsinki: Helsinki University Printing House).

Lauren, J., Airaksinen, M.S., Saarma, M., and Timmusk, T. (2003). A novel gene family encoding leucine-rich repeat transmembrane proteins differentially expressed in the nervous system. Genomics *81*, 411–421.

Levinson, J.N., Chery, N., Huang, K., Wong, T.P., Gerrow, K., Kang, R., Prange, O., Wang, Y.T., and El-Husseini, A. (2005). Neuroligins mediate excitatory and inhibitory synapse formation: involvement of PSD-95 and neurexin-1beta in neuroligin-induced synaptic specificity. J. Biol. Chem. *280*, 17312–17319.

Lin, J.C., Ho, W.H., Gurney, A., and Rosenthal, A. (2003). The netrin-G1 ligand NGL-1 promotes the outgrowth of thalamocortical axons. Nat. Neurosci. *6*, 1270–1276.

Linhoff, M.W. (2008). Expression Screening for Proteins Involved in CNS Presynaptic Differentiation and Initial Characterization of the Synaptogenic LRRTM Protein Family (St. Louis: Washington University in St. Louis).

Majercak, J., Ray, W.J., Espeseth, A., Simon, A., Shi, X.P., Wolffe, C., Getty, K., Marine, S., Stec, E., Ferrer, M., et al. (2006). LRRTM3 promotes processing of amyloid-precursor protein by BACE1 and is a positional candidate gene for late-onset Alzheimer's disease. Proc. Natl. Acad. Sci. USA *103*, 17967–17972.

Micheva, K.D., and Beaulieu, C. (1996). Quantitative aspects of synaptogenesis in the rat barrel field cortex with special reference to GABA circuitry. J. Comp. Neurol. *373*, 340–354.

Missler, M., Zhang, W., Rohlmann, A., Kattenstroth, G., Hammer, R.E., Gottmann, K., and Sudhof, T.C. (2003). Alpha-neurexins couple Ca2+ channels to synaptic vesicle exocytosis. Nature *424*, 939–948.

Nishimura-Akiyoshi, S., Niimi, K., Nakashiba, T., and Itohara, S. (2007). Axonal netrin-Gs transneuronally determine lamina-specific subdendritic segments. Proc. Natl. Acad. Sci. USA *104*, 14801–14806.

Paradis, S., Harrar, D.B., Lin, Y., Koon, A.C., Hauser, J.L., Griffith, E.C., Zhu, L., Brass, L.F., Chen, C., and Greenberg, M.E. (2007). An RNAi-based approach identifies molecules required for glutamatergic and GABAergic synapse development. Neuron *53*, 217–232.

Rodriguez, I., Feinstein, P., and Mombaerts, P. (1999). Variable patterns of axonal projections of sensory neurons in the mouse vomeronasal system. Cell *97*, 199–208.

Scheiffele, P., Fan, J., Choih, J., Fetter, R., and Serafini, T. (2000). Neuroligin expressed in nonneuronal cells triggers presynaptic development in contacting axons. Cell *101*, 657–669.

Sheng, M., and Sala, C. (2001). PDZ domains and the organization of supramolecular complexes. Annu. Rev. Neurosci. *24*, 1–29.

Shibata, Y., Carninci, P., Watahiki, A., Shiraki, T., Konno, H., Muramatsu, M., and Hayashizaki, Y. (2001). Cloning full-length, cap-trapper-selected cDNAs by using the single-strand linker ligation method. Biotechniques *30*, 1250–1254.

Stevens, B., Allen, N.J., Vazquez, L.E., Howell, G.R., Christopherson, K.S., Nouri, N., Micheva, K.D., Mehalow, A.K., Huberman, A.D., Stafford, B., et al. (2007). The classical complement cascade mediates CNS synapse elimination. Cell *131*, 1164–1178.

Tabuchi, K., Blundell, J., Etherton, M.R., Hammer, R.E., Liu, X., Powell, C.M., and Sudhof, T.C. (2007). A neuroligin-3 mutation implicated in autism increases inhibitory synaptic transmission in mice. Science *318*, 71–76.

Varoqueaux, F., Jamain, S., and Brose, N. (2004). Neuroligin 2 is exclusively localized to inhibitory synapses. Eur. J. Cell Biol. *83*, 449–456.

Varoqueaux, F., Aramuni, G., Rawson, R.L., Mohrmann, R., Missler, M., Gottmann, K., Zhang, W., Sudhof, T.C., and Brose, N. (2006). Neuroligins determine synapse maturation and function. Neuron *51*, 741–754.

Waites, C.L., Craig, A.M., and Garner, C.C. (2005). Mechanisms of vertebrate synaptogenesis. Annu. Rev. Neurosci. *28*, 251–274.

Wang, C.Y., Chang, K., Petralia, R.S., Wang, Y.X., Seabold, G.K., and Wenthold, R.J. (2006). A novel family of adhesion-like molecules that interacts with the NMDA receptor. J. Neurosci. *26*, 2174–2183.

Yamagata, M., Sanes, J.R., and Weiner, J.A. (2003). Synaptic adhesion molecules. Curr. Opin. Cell Biol. *15*, 621–632.